Formation of Ion Irradiation Induced Small-Scale Defects on Graphite Surfaces

K. Nordlund and J. Keinonen
Accelerator Laboratory, University of Helsinki, P.O. Box 43, FIN-00014 Helsinki, Finland

T. Mattila
Laboratory of Physics, Helsinki University of Technology, FIN-02150 Espoo, Finland
(Received 17 April 1996)

We use molecular dynamics simulations and *ab initio* calculations to study the structures and formation probabilities of isolated surface defects produced by ion irradiation of (1000) graphite. We improve the conventionally used Tersoff potential [J. Tersoff, Phys. Rev. Lett. **61**, 2879 (1988)] to realistically describe interlayer forces in graphite and high-energy processes in carbon. We identify three defect structures which correspond to experimentally observed hillocks on graphite surfaces, and examine their formation at different implantation energies. [S0031-9007(96)00757-0]

PACS numbers: 68.35.Dv, 34.20.Cf, 61.80.Jh

The (1000) surface of graphite is peculiar in that carbon atoms are arranged in planar layers with strong covalent bonding within planes parallel to the surface, but only weak residual bonding between the planes. Many aspects of ion irradiation induced damage on graphite surfaces have been the subject of much interest recently [1–6]. Despite the extensive experimental work it is still, to a large extent, unclear what atomic structures and formation mechanisms are the source of observed defect and damage structures.

In this Letter, we use molecular dynamics (MD) simulations and *ab initio* calculations to study the formation of the small-scale defects comprising a few tens of atoms frequently seen in scanning tunneling microscopy (STM) and atomic force microscopy (AFM) measurements of ion-irradiated graphite surfaces [5–9]. Typically, they take the form of hillocks (bumps) in which the regular lattice seen in STM measurements is raised 1–10 Å from its surroundings. The number and location of the electronic protrusions in hillocks usually remain unchanged from that of undisturbed lattice regions.

We identify atomic structures which correspond to the small-scale defects seen in the experiment. Our study of defect formation mechanisms and probabilities shows that vacancies are the predominant source of defects, but that clusters of interstitial atoms between the surface and second graphite plane also occur in significant numbers. Furthermore, we identify a defect structure in which an extra atom has entered a stable position in the surface graphite layer, forming a triangular threefold ring. Recent results show that carbon may occur in an even greater multitude of forms and bonding types than previously known in clusters and the amorphous state [10,11]. Our results suggest that unusual bonding types may occur on bulk graphite layers as well.

Classical molecular dynamics simulations are the most realistic methods available within the limits of current computer capacity for studying ion irradiation processes dynamically. In them, it is essential to use a good interatomic potential. Although several potentials which describe carbon in its graphite form have been presented in the literature [12–15], we found that none of them describes graphite in a manner suitable for our needs. To provide a firm foundation for our study, we formulated a potential which enables practical MD simulations of energetic processes in graphite.

The Tersoff potential [12,16] much used in the literature (see, e.g., Refs. [17–19]) is based on a relatively wide range of data and gives a good description of the covalent bonds in many forms of carbon, including graphite. However, due to its short range (2.1 Å), it does not describe the weak interactions between graphite planes, which lie 3.35 Å from each other [20]. We developed an improvement of the Tersoff potential which retains the good description of the covalent bonding, yet also describes accurately both the short-range repulsive part of the potential and the long-range bonding between graphite planes.

The potential parameters were fit to several sets of data. These were an experimentally determined force function between layers [21], graphite-to-diamond phase transition data [22] (to provide for a good description of strong distortions of the lattice structure in collision cascades), and a realistic repulsive potential obtained from density-functional theory (DFT) calculations using the local density approximation (LDA) [23,24]. To confirm that the advantageous properties of the Tersoff potential are not lost, we reproduced the cohesive energies in and near equilibrium and the equilibrium total energies and bond lengths for the diamond, graphite, and dimer structures.

To obtain a good fit to the graphite-to-diamond phase transition, the Tersoff potential parameter λ_3 was set equal to μ (λ_2) as in Ref. [16]. Also, the high-end cutoff S was optimized to the value $S = 2.46$ Å. Otherwise, the values of the Tersoff potential parameters are as in Ref. [12] (the parameter notation used here is the same as in Ref. [25]).

Our potential has the following functional form:

 © 1996 The American Physical Society

$$\phi_1(\theta_{ijk}) = \frac{1}{1 + (\cos\theta_{ijk}/l_1)^4}, \quad \phi_2(r_{ik}) = \frac{1}{1 + [(r_{ik} - r_0)/l_2]^4},$$
$$G_{ij} = \sum_{k \neq i,j} \phi_1(\theta_{ijk})\phi_2(r_{ik}), \quad \phi_3(G_{ij}) = -\frac{l_0}{1 + [(G_{ij} - 3)/l_3]^2},$$
$$V_G(r_{ij}) = \phi_3(G_{ij})[V_{c_0} - (e^{-l_4(r_{ij}-c_0)} - 1)^2],$$

where r_{ij} is the distance between atoms i and j and θ_{ijk} is the angle between atoms i, j, and k as seen from atom i. The final graphite potential function V_G is obtained by multiplying the bonding term ϕ_3 with a Morse potential corresponding to the experimental interlayer force [21].

To prevent our potential function from interfering with the Tersoff potential, we use a low-end cutoff for V_G at $r_{M,0} = c_0 - \ln(1 + \sqrt{V_{c_0}})/l_4$, where $V_G = 0$. For efficient MD simulations we use also a high-end cutoff $r_{M,1}$.

The *ab initio* repulsive potential V_R is obtained by doing a spline interpolation of data points obtained at dense r_{ij} intervals from DFT and LDA calculations [26]. The repulsive potential is smoothly fitted with the Tersoff potential V_T using a Fermi function $F(r) = (1 + e^{-b_f(r-r_f)})^{-1}$. The final potential is

$$V(r) = V_R(r)[1 - F(r)] + [V_G(r) + V_T(r)]F(r).$$

The parameter values $r_0 = 1.46$ Å, $c_0 = 3.348$ Å, $l_0 = 0.0456$ eV, and $l_4 = 1.94$ Å^{-1} are determined directly from experimental data [20,21]. The fitting procedure resulted in the values $l_1 = 0.07$, $l_2 = 0.21$ Å, $l_3 = 0.15$, $V_{c_0} = 2.33$, $r_{M,1} = 4.3$ Å, $b_f = 14$ Å^{-1}, and $r_f = 0.95$ Å.

The fit of the potential to the experimental interplanar energy vs distance curve [21] is shown in Fig. 1, and the fit to the diamond-to-graphite transition energy curve is shown in Fig. 2. A good fit is obtained in both cases. Near-equilibrium properties of carbon and defect energies of the in-plane defects in graphite are not modified significantly from the good description given by the original Tersoff potential [12]. For the interplane interstitial our potential gave the formation energy 5.8 eV, which compares well with the experimental value 7.0 ± 1.5 eV [27].

Our potential gave a firm basis for studying damage production on graphite surfaces. Extensive studies of ion-irradiation-induced defects on graphite surfaces [5–9] have not unambiguously shown what atomic structures are the source of the experimentally seen small-scale defects. Since STM measurements of graphite surfaces show one protrusion in the observed electronic density per two surface atoms, it is difficult to deduce the atomic structure based on experiment alone. Several authors have studied graphite surface erosion processes using MD simulations (see, e.g., Refs. [17,28]), but there has been no systematic study on the formation probability and final structure of surface defects. In this Letter, we collect representative statistics from MD simulations to obtain a quantitative view of the defect formation processes.

Very recently Hahn *et al.* have shown that vacancies on the graphite surface can appear as surface protrusions in STM measurements [5]. Some of the hillocks seen in experiment are caused by impurity atoms between the surface and second layer of atoms in graphite [5,7]. However, hillocks also occur during self-ion-implantation [8], and one incident atom may cause the formation of several hillocks [6]. Thus, in many cases the formation of hillocks involves only carbon atoms.

Our MD simulations are based on the usual microcanonical formalism. We use the ZBL electronic stopping power [29] to treat the inelastic energy loss of energetic atoms. The simulation cell consists of 2000–3000 atoms arranged so that the parts of the collision cascade affecting the surface are contained within the cell borders. The

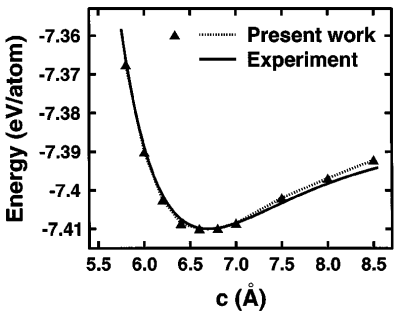

FIG. 1. Total energy per atom of graphite as a function of the graphite lattice c parameter. The solid line shows the experimental curve, the triangles and dotted line result from our potential.

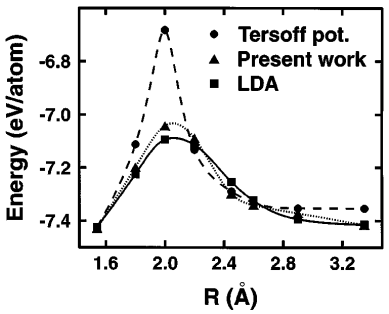

FIG. 2. Total energy per atom of the diamond to rhombohedral graphite transformation as a function of the interlayer distance R parameter. The squares show the energy given by *ab initio* calculations in Ref. [22], the circles the result of the original Tersoff potential, and the triangles the result of our potential. The lines are drawn to guide the eye.

temperature of the atoms near the cell border is scaled down to 300 K during the simulation to dissipate kinetic energy out of the simulation cell.

At least 200 recoil events were simulated for each type of initial recoil condition to obtain representative statistics of the defect formation processes. To obtain the equilibrium atomic configuration, the temperature of the simulation cell was quenched down to 0 K after the collision cascade had thermalized. We verified that the defect types produced in the simulations are stable for at least 3 ps after the thermalization of the collision cascade and that the quench does not change the defect structure.

To study the effect of low-energy ion implantation on defect production, we simulated 100 eV–3 keV carbon recoils incident on the (1000) graphite surface, aligned 65° from the [1000] axis towards the [0100] axis (cases 1–3 in Table I). To study defects formed by secondary recoils in high-energy implantations (cf., e.g., Ref. [6]), we simulated secondary recoils with energies 100 eV–3 keV. These were modeled by placing an extra atom between the third and fourth layers in graphite, and giving it an initial direction towards the surface chosen isotropically in the solid angle cone defined by the [1000] and [1300] crystal directions (cases 4–7 in Table I).

Since STM and AFM measurements probe the electronic structure of the defects, we also performed DFT and LDA calculations to obtain the electronic structures of the defect types which we found to occur in statistically significant numbers in the MD simulations. The electronic wave functions were expanded in the plane-wave basis, and a 20 Ry kinetic energy cutoff was found to give well converged results with Vanderbilt-type pseudopotentials [30]. Supercells containing up to 51 atoms were applied and full atomic relaxations were allowed. The DFT calculation method we use is among the best ones available for these types of problems within the limits of current computer capacity, and has been found to yield good correspondence between surface electronic structure and experiment by other authors [31].

TABLE I. Average number of different types of defects produced on the graphite surface by one recoil atom. Cases 1–3 denote implantation of a recoil incident on graphite, cases 4–7 secondary recoils. *N* denotes the number of events simulated. SV denotes single vacancies in the graphite surface layer, CV divacancy, trivacancy, etc. vacancies, and groups of nearby single vacancies and SI single interstitial atoms between the surface and second layer.

Implantation case	*N*	Defects/recoil atom SV	CV	SI	*D*3
1. 300 eV inc.	264	0.62	0.15	0.55	0.0
2. 1 keV inc.	255	0.43	0.54	1.14	0.02
3. 3 keV inc.	220	0.63	0.30	0.96	0.04
4. 100 eV sec.	204	0.0	0.0	0.61	0.005
5. 300 eV sec.	309	0.31	0.06	0.74	0.06
6. 1 keV sec.	240	0.46	0.17	0.56	0.02
7. 3 keV sec.	201	0.29	0.11	0.31	0.005

From our MD simulations we identified three main types of surface defects occurring in statistically significant numbers. These were surface vacancies, interplane interstitials below the surface layer, and *D*3 defects (see below). These defect structure types accounted for more than 99% of all defects produced.

For vacancies, our *ab initio* calculations revealed that no considerable change in the total valence electron density is connected to the missing atom site when compared with the ideal structure. However, we found that the partial charge density which originates from the states close to the Fermi energy is enhanced at the atoms surrounding the vacancy. These results are in a good agreement with those of Hahn *et al.* [5], who state that vacancies are not observable by AFM but appear as protrusions in STM.

The carbon single interstitial between planes is mobile at room temperature [27] and cannot therefore be the source of hillocks. However, the single interstitials may migrate to form dimers and clusters between the layers [32], which may be the source of some of the hillocks. Interstitials do not annihilate with vacancies in significant numbers at room temperature [27,32]. Using our interatomic potential we found that an interlayer dimer and trimer produce relatively low and broad hillocks, with atomic heights of 0.7 and 1.0 Å, and volumes corresponding to roughly 5 and 14 atomic volumes, respectively. Computer capacity limitations prevented us from studying interstitials using *ab initio* methods.

Since defect migration occurs on relatively long time scales, the formation of clusters cannot be simulated using molecular dynamics simulations. However, an upper bound for their number can be obtained by dividing the number of single interstitials by two.

In addition to vacancies and interstitials, we also found a surface defect where an extra atom has entered the top layer, resulting in a threefold coordinated vertical ring (Fig. 3). We label this defect type "*D*3." The topmost atom is about 2 Å higher than the undisturbed lattice, and its neighboring atoms have risen significantly from the surroundings. The triangle formed by the threefold ring is nearly equilateral, with lengths 1.49 Å for the upward bonds and 1.56 Å for the horizontal bond. The threefold bonding of the *D*3 defect bears similarity to bonding orbital types seen very recently in *ab initio* calculations of amorphous carbon [11] and emphasizes the ability of carbon to exist in a variety of stable bonding configurations.

Inspection of collision cascades showed that the structure can be formed by a single low-energy ($E \sim 50$ eV) recoil atom incident on the surface layer from below, displacing an atom in a graphite ring which then enters an interstitial site.

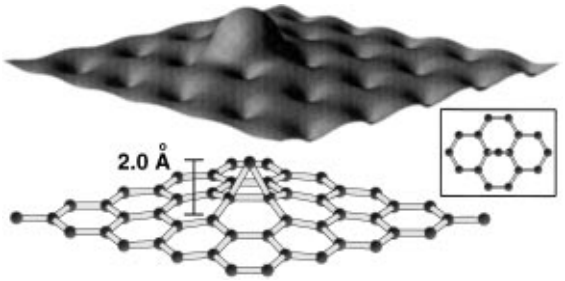

FIG. 3. Atomic and electronic structure of the $D3$ defect identified in our simulations. The constant-value surface corresponds to a valence electron density of $0.02e/\mathrm{bohr}^3$. To provide a clear view of the atomic structure, the electron density has been raised in the figure. The inset shows the defect viewed from above the graphite (1000) surface.

The *ab initio* calculations verified that the $D3$ defect structure is stable and gave a binding energy of -3.3 eV for it. Both the valence electron density and the partial charge density of the uppermost occupied orbital have strong maxima above the top atom in the defect (Fig. 3), which indicates that the structure appears as a hillock in AFM and STM measurements, with a height of at least 2 Å. We suggest that $D3$ defects may be the source of some of the hillocks higher than 2 Å reported in the literature [9].

In Table I we present the relative formation probabilities obtained for the defect types presented above. From the table we see that, in the case of *incident* recoils, vacancies and single interstitials occur in roughly equal numbers. Taking into account that single interstitials must form clusters to produce visible hillocks at room temperature, we see that vacancies are the dominant source of hillocks in low-energy ion implantation. The $D3$ defects account for $(0-3)\%$ of the observable defects.

Secondary recoils (cases 4–7 in the table) form significantly more single than complex vacancies at all energies. The lower energy secondary recoils (cases 4 and 5) are likely to be stopped within the graphite lattice, and therefore form more interstitial atoms, whereas the higher energy secondary recoils form more vacancies. Again, taking interstitial clustering into account, we see that vacancies are the dominant source of defects. Secondary recoils with energies of a few hundred eV (occurring frequently during high-energy ion implantation) also have a significant contribution of $D3$ defects.

In conclusion, we have constructed a new interatomic potential especially well suited for molecular dynamics simulations of graphite and high-energy processes in carbon. We have studied the formation mechanisms and structures of different types of defects and discussed their correspondence to experimental STM and AFM results. We found that the predominant source of small-scale hillocks seen in STM measurements are single and complex vacancies and that, at most, half of the defects may be formed by interstitial atom clusters. We further identified a surface defect in which an extra atom has entered the surface layer in a threefold bonding structure, which we suggest may be the source of some of the hillocks seen in the experiment.

[1] G. Galli and F. Mauri, Phys. Rev. Lett. **73**, 3471 (1994).
[2] R. A. Spits, J. F. Prins, and T. E. Derry, Nucl. Instrum. Methods Phys. Res., Sect. B **85**, 347 (1994).
[3] L. Begrambekov, S. Vergazov, A. Zakharov, and M. Morochev, Nucl. Instrum. Methods Phys. Res., Sect. B **90**, 491 (1994).
[4] I. Koponen and M. Hautala, Nucl. Instrum. Methods Phys. Res., Sect. B **103**, 156 (1994).
[5] J. R. Hahn, H. Kang, S. Song, and I. C. Jeon, Phys. Rev. B **53**, R1725 (1996), and references therein.
[6] K. P. Reimann, W. Bolse, U. Geyer, and K. P. Lieb, Europhys. Lett. **30**, 463 (1994).
[7] D. Marton *et al.,* Surf. Sci. **326**, L489 (1995).
[8] R. Coratger, A. Claverie, F. Ajustron, and J. Beauvillain, Surf. Sci. **227**, 7 (1990).
[9] L. Porte *et al.,* Nucl. Instrum. Methods Phys. Res., Sect. B **44**, 114 (1989).
[10] J. C. Grossman, L. Mitas, and K. Raghavachari, Phys. Rev. Lett. **75**, 3870 (1995).
[11] G. Ackland (private communication).
[12] J. Tersoff, Phys. Rev. Lett. **61**, 2879 (1988).
[13] M. I. Heggie, J. Phys. Condens. Matter **3**, 3065 (1991).
[14] J. R. Chelikowsky, Phys. Rev. B **45**, 12 062 (1992).
[15] E. P. Andribet *et al.* (to be published).
[16] J. Tersoff, Phys. Rev. B **37**, 6991 (1988).
[17] R. Smith and R. P. Webb, Nucl. Instrum. Methods Phys. Res., Sect. B **59/60**, 1378 (1991).
[18] T. Mattila and R. M. Nieminen, Phys. Rev. Lett. **74**, 2721 (1995).
[19] D. B. Boercker, Phys. Rev. B **44**, 11 592 (1991).
[20] R. Wyckoff, Crystal Structures (Interscience, New York, 1948), Chap. II, p. 11.
[21] D. P. DiVincenzo, E. J. Mele, and N. A. W. Holzwarth, Phys. Rev. B **27**, 2459 (1983).
[22] S. Fahy, S. G. Louie, and M. L. Cohen, Phys. Rev. B **34**, 1191 (1986).
[23] J. Keinonen *et al.,* Nucl. Instrum. Methods Phys. Res., Sect. B **88**, 382 (1994).
[24] K. Nordlund, D. Sundholm, and N. Runeberg (to be published).
[25] J. Tersoff, Phys. Rev. B **39**, 5566 (1989).
[26] The repulsive potential data are available by electronic request from kai.nordlund@helsinki.fi.
[27] P. A. Thrower and R. M. Mayer, Phys. Status Solidi (a) **47**, 11 (1978).
[28] A. Gras-Martí *et al.,* Comput. Mater. Sci. **3**, 413 (1995).
[29] J. F. Ziegler, J. P. Biersack, and U. Littmark, *The Stopping and Range of Ions in Matter* (Pergamon, New York, 1985).
[30] D. Vanderbilt, Phys. Rev. B **41**, 7892 (1990); K. Laasonen *et al.,* Phys. Rev. B **47**, 10 142 (1993).
[31] R. B. Capaz, K. Cho, and J. D. Joannopoulos, Phys. Rev. Lett. **75**, 1811 (1995).
[32] H. Maeta, T. Iwata, and S. Okuda, J. Phys. Soc. Jpn. **39**, 1558 (1975).